Magnetic tunnel junctions with MgO-EuO composite tunnel barriers

Guo-Xing Miao and Jagadeesh S. Moodera

Phys. Rev. B **85**, 144424 — Published 24 April 2012

DOI: 10.1103/PhysRevB.85.144424

Magnetic Tunnel Junctions with MgO-EuO composite tunnel barriers

Guo-Xing Miao[1,2*], Jagadeesh S. Moodera[1]

1. Francis Bitter Magnet Laboratory, Massachusetts Institute of Technology, Cambridge, MA 02139 USA

2. Institute for Quantum Computing, University of Waterloo, Waterloo, ON N2L3G1 CANADA

The chalcogenide compound EuO is best known as a highly efficient spin-filter tunnel barrier material. Using molecular beam epitaxy method, we combine polycrystalline EuO with epitaxial MgO and construct magnetic tunnel junctions with such hybrid tunnel barriers. Tunnel magnetoresistance of over 40% was achieved in junctions with oxygen-rich EuO. For lower oxygen concentration, magnetoresistance decreases dramatically and eventually vanishes, indicating that spin-filtering is weakened when the transport is mainly mediated by excess conduction channels through defect sites.

Shortly after the discovery of room temperature tunnel magnetoresistance (TMR) in the mid-1990s [1,2], this field witnessed significant boom in terms of both fundamental science and technological applications. Various approaches have been explored in order to enhance the TMR value, for example, incorporate half-metallic electrodes for their near ideal spin polarizations [3,4,5], to construct epitaxial MgO barriers coupled with bcc-ferromagnets for the establishment of coherent tunneling [6,7,8,9], or to take advantage of magnetic insulators for their spin-filter capabilities [10,11,12,13]. Tremendous progress has been made with these approaches for the purpose of generating and enhancing TMR [14]. In this article, we construct a hybrid tunnel barrier to combine MgO's symmetry-filter property, which has witnessed tremendous success in industry, together with EuO's spin-filter property. Both symmetry-filtering and spin-filtering are known to produce nearly 100% spin polarization in the tunnel current, thus such a combination could in principle lead to significant enhancement in the achievable TMR ratios. In addition, changing EuO magnetization would lead to the observation of a giant TMR without a ferromagnetic counter electrode on the top. Experimentally, however, we found that the resultant TMR ratio is modest, and falls roughly in the range expected from the spin polarizations of Fe/MgO and EuO. The stoichiometry of EuO turned out to play an important role in determining the transport properties of these magnetic tunnel junctions (MTJs). The continued optimization of spin-filter materials, and search for more suitable candidates, will remain a challenge in this field.

The sample stacks studied in this work were prepared in a molecular beam epitaxy system (MBE) with the base pressure at 1×10^{-10} torr. We used HF etched (100)-Si

wafers as the substrates. To seed the (100) oriented epitaxial growth of bcc-Fe, a 5 nm MgO buffer layer was firstly laid down at 300°C, and the Fe bottom electrode and MgO tunnel barrier were subsequently deposited at 180°C. The samples were then cooled down to room temperature for EuO growth. We stabilized the oxygen pressure ($1\sim10\times10^{-8}$ torr) inside the chamber by modulating the oxygen flow through a needle valve before starting the Eu flux, which was kept constant at 1.4 nm/min for all the samples (corresponding to a nominal EuO growth rate of 1.0 nm/min). We immediately stopped the oxygen flow after 3 nm EuO deposition and capped the samples with 3 nm Y. They were then *in-situ* transferred to a magnetron sputtering chamber and further capped with 50 nm Al. Finally, 3 nm Cr / 5 nm Au was placed on top by MBE to facilitate top contacts for micro-fabrication processes. No post-annealing was performed on these MTJ stacks. The wafers were then patterned with optical lithography with the junction areas about 80×80 μm^2, and the transport measurement was done at 1 K in a pumped He^4 reservoir. X-ray diffraction (XRD) and magnetic measurement were performed in a Rigaku diffractometer and a Quantum Design Superconducting Quantum Interference Device magnetometer (SQUID), respectively. EuO films for magnetic characterization are nominally 5nm thick, and directly deposited on HF-etched Si substrates then capped with 3 nm Y and 50 nm Al.

I. Magnetic properties of EuO films

We start by examining the magnetic properties of as-deposited EuO films. EuO is a ferromagnetic insulator with its bulk Curie temperature (T_C) at 69 K. our films were deposited under different oxygen pressures with a fixed Eu flux rate, and the total

deposited Eu amount is equivalent to that of a 5 nm stoichiometric EuO film. The saturation moment of the films shows a generic trend (Fig.1): it peaks at an optimized oxygen pressure (~ 4×10^{-8} torr), and decreases for both over- and under-oxidized films. This trend can be easily understood. For Eu-rich films, the excess Eu atoms tend to form antiferromagnetic ordering among themselves without the ferromagnetic exchange interaction mediated through O bonds (Eu metal is a helical antiferromagnet with Neel temperature ~91 K and helical pitch ~1.6 nm [15]), therefore the total measured magnetic moment is reduced. On the other hand, when the EuO films are oxygen-rich, it partially forms the more stable Eu_2O_3 phase which is a nonmagnetic insulator and does not contribute to the measured magnetization either. From the above analysis, we can see that the maximum saturation moment, normalized to each Eu atom, should correspond to the optimized EuO growth condition with the resultant films closest to stoichiometry.

Here we attempt to address the large scattering in the measured data points in Fig.1. The average magnetic moment of Eu atoms (the y-axis) carries uncertainty associated with the determination of the Eu flux, the sample area, and the saturation magnetic moment. These experimental errors are relatively minor and do not contribute significantly to the data scattering. The major challenge in the sample preparation was the control of oxygen pressure before and during the film growth. To enhance reproducibility, we gave the system more than enough time (2 hours) to stabilize the oxygen pressure before starting the EuO growth. We found that if we waited for shorter time, such as one hour, the sample reproducibility from run to run became significantly deteriorated. This is largely due to the high reactivity of Eu metal with oxygen gases. When the inner chamber walls of MBE are coated with under-oxidized Eu or Eu^{2+} from previous depositions,

these coatings function as strong pumps for oxygen molecules and can alter the gas flow distribution inside the chamber significantly. We thus settled the gas pressure for a long time in order to saturate the chamber and to establish a very well-defined starting condition before the EuO growth. As soon as the Eu flux was started, the system pressure decreased dramatically by a factor of 2~5 depending on the starting pressure, indicating that the Eu flux were effectively reacting with oxygen on the fly. The actual during-growth pressure turned out to be a non-equilibrium parameter, varied greatly over the course of growth and hard to manipulate reproducibly. The data reported in this article are therefore plotted against the initial chamber pressure before the Eu flux is turned on. Our data suggest that oxygen pressure in the range of $3\sim4\times10^{-8}$ torr is the optimized condition for the EuO growth at the given growth rate.

We next take a look at the magnetic properties of a few characteristic films, grown at largely distinct background oxygen pressures (Fig.2). The average magnetic moment is approximately 6 μ_B/Eu for the optimally oxidized film, grown at $P_{Oxygen} \sim 4\times10^{-8}$ torr, slightly lower than the theoretical value of 7 μ_B/Eu with Eu in its $[Xe]4f^7$ (Eu^{2+}) electronic configuration. The non-ideal magnetization is probably due to the degraded top and bottom EuO interfaces, which absorb excess oxygen and form Eu^{3+} for a monolayer or two. On the other hand, the measured T_C is very close to its bulk value of 69 K confirming the good quality of these films. For over- and under-oxidized films grown at P_{Oxygen} = 7.0 and 1.8×10^{-8} torr respectively, their magnetic moments are reduced, more so on the over-oxidized films. As discussed earlier, this is because of the formation of Eu and Eu_2O_3 phases, neither of which is ferromagnetic. One unique feature observed for the Eu-rich film is that its T_C is elevated beyond the bulk value. Improvement of T_C

with electron doping has long been reported in EuO [16] and attributed to the carrier enhanced indirect exchange interactions [17].

II. Magnetic tunnel junctions with MgO/EuO hybrid barriers

After examination of the general magnetic properties of EuO thin films, we proceeded to integrate them into MTJ stacks. The epitaxial growth of bcc-Fe/MgO on (100)-Si was well optimized before [18]. X-ray diffraction on the hybrid MTJ stacks (Fig.3) showed clear (100)-Fe peak, and the (100)-MgO only showed up as a broad bump due to its ultra-small thickness. In addition to functioning as a symmetry-filter to promote coherent tunneling, the MgO layer also serves as a spacer layer between Fe and EuO to eliminate any direct exchange coupling [19,20]. The lattice parameters of the few common Eu-O phases are, respectively, 5.142 Å for EuO, 4.578 Å for Eu, and 10.86 Å for cubic Eu_2O_3. None of these is trivially lattice-matched with the epitaxial (100)-MgO surface, whose lattice spacing is 4.211 Å. Elevated temperature are necessary to establish epitaxial correlation between these systems, for example, between EuO and MgO [21,22]. Because of room temperature deposition in our case, the EuO layer is polycrystalline and most pronounced in the (111) and (100) orientations. Our choice of room temperature growth is for the ease of tuning oxygen concentration while still keeping the layer thickness in the nm ranges, because ultra-thin EuO films suitable for barrier applications tend to degrade very rapidly in oxygen environment if heated, immediately after the growth termination. This is less an issue for studies based on more bulk-like EuO films. Our deposited EuO is mostly (100)-oriented when close to stoichiometry (Fig.3b), because this is its preferred alignment with respect to the (100)-MgO surface [21,22]. The

oxygen rich EuO turns out to be more (111)-oriented (Fig.3c), probably because of the complications from appearance of the Eu_2O_3 phases. For films deposited in very low oxygen pressure a well pronounced Eu (110) peak develops (Fig.3a), indicating the appearance of metallic Eu in such films.

Next we focus on the electrical transport across these MTJs. Fig.4 shows an example of the observed TMR and its bias dependence for a junction with EuO deposited at oxygen pressure of 6×10^{-8} torr, ie., slightly over-oxidized. The sharp resistance increase at smaller field magnitude corresponds to the switching of the bottom Fe layer, while the more gradual resistance decrease at larger fields corresponds to the switching of the spin-filter EuO layer (Fig.4b). EuO switching tends to be more rounded at higher oxygen concentration, as readily seen in Fig.2a. TMR in these devices reached over 40%, in line with what's expected from a simple estimate from the spin polarizations. For Fe/MgO/Fe MTJs, we obtained TMR of 195% at 1 K [18], corresponding to a spin polarization of 70% for the epitaxial Fe/MgO combination. For EuO tunnel barriers, spin polarization of 29% was directly probed by the superconducting Meservey-Tedrow technique [23]. Combining these known numbers into the simple Julliere's model, the expected TMR would be around 50% across the MgO/EuO hybrid tunnel barriers, quite comparable with what we obtained here. The slightly lower TMR we measured experimentally is probably due to the less than ideal magnetic alignment between the Fe and EuO layers. As one can see in Fig.4b, the antiparallel configuration does not show up as a flat plateau in the R-H curve, indicating that partial EuO switching (as seen in Fig.2a, the very broad switching) already happens before Fe switches, therefore reduces the maximum achievable TMR. We take this broadening of magnetic switching as evidence

that the films break into finer crystals/domains in the presence of Eu_2O_3, which have more significant distributions in their crystal properties and are also more subject to thermal influences. This is further evidenced with the reduction and broadening of the overall T_C (Fig.2b).

The TMR bias dependence showed clear signature of the spin-filter tunneling. As a function of bias voltage, TMR shows a very pronounced peak on each bias polarity, corresponding to the onset of Fowler-Nordheim (F-N) tunneling [24]. That is, when the applied bias voltage is higher than the spin-filter tunnel barrier height, the electrons can then hop across the barrier by field emission and the tunnel current is significantly increased. In the case of spin-filter tunnel barrier, when one of its spin channels establishes F-N tunneling, the other channel still has not. This results in an enhancement of the tunnel spin polarization thus an enhanced TMR at certain bias voltages [25]. For very low bias voltages (shaded area), we could not obtain reasonable measurement due to the high junction impedance in this range (> 1 GΩ).

When the EuO layers were deposited using the optimized oxygen pressure (~ 4×10^{-8} torr), the TMR is however lower and shows different bias behavior (Fig.4 inset). Resistances of these junctions are a factor of 3 lower compared to that of the junctions grown at 6×10^{-8} torr oxygen pressure, suggesting additional electron conduction channels are opened. The enhancement of TMR with F-N tunneling is essentially washed out, and the resultant bias dependence looks more similar to a traditional MTJ constructed from metallic electrodes. This is clear evidence that when EuO is magnetically optimized on average, it still contains lots of defect levels inside (mediated by excess Eu atoms/clusters). These defect levels have strong moments (7 μ_B at $[Xe]4f^7 6s^2$) but are not

ferromagnetically ordered like their Eu^{2+} counterparts, and they allow for charge transport that is mildly spin-dependent at best, thus leads to the weakened TMR. These barriers are also more conductive because the electrons tend to flow across these defect levels rather than tunnel across the barrier, thus EuO is not a proper spin-filter barrier in this case, but closer to a metallic electrode. With further reduction in the EuO growth pressure, for example, to 3×10^{-8} torr, the junctions showed much higher conductance and no noticeable TMR was observed. This is understandable because the dramatic increase in junction conductance (more than two orders of magnitude difference between devices made at 3×10^{-8} torr and those made at 6×10^{-8} torr) is dominated by unpolarized electron transport, thus the TMR drops to essentially zero. On the other hand, defect states are readily filled up in slightly over-oxidized EuO films and spin-filtering is restored to its optimum electrical performance. For even more oxidized EuO films, there is significant presence of Eu_2O_3. Eu^{3+} is nonmagnetic (0 μ_B at $[Xe]4f^6$) thus does not scatter spins much, however, they do not contribute to spin-filtering either. Patches of Eu_2O_3 thus reduce the spin-filter efficiency. In addition, Eu_2O_3 is a much better insulator with a much broader band gap compared to EuO, as a result junction impedence at higher oxygen concentration increases dramatically and becomes increasingly harder to measure. Similar trends were also reported in [23].

In summary, we have studied the magnetic properties of EuO reactively deposited in an MBE environment, and used the knowledge to build MTJs consisting of MgO/EuO hybrid tunnel barriers. Slight over-oxidation in EuO films helps reducing defect levels within the barrier and leads to better spin-filter performance.

The authors wish to thank the following grants for supporting this work, NSF DMR 0504158 and ONR N00014-09-1-0177.

*Correspondence: gxmiao@mit.edu

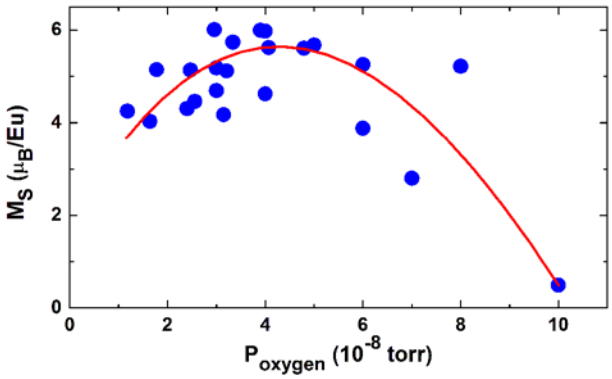

Fig.1 Normalized saturation magnetization of EuO thin films as a function of the initial oxygen pressure before the reactive deposition. All films were deposited on HF cleaned Si substrates, with nominal thickness of 5 nm and capped with 3 nm Y / 50 nm Al. Solid line is for visual guidance purpose.

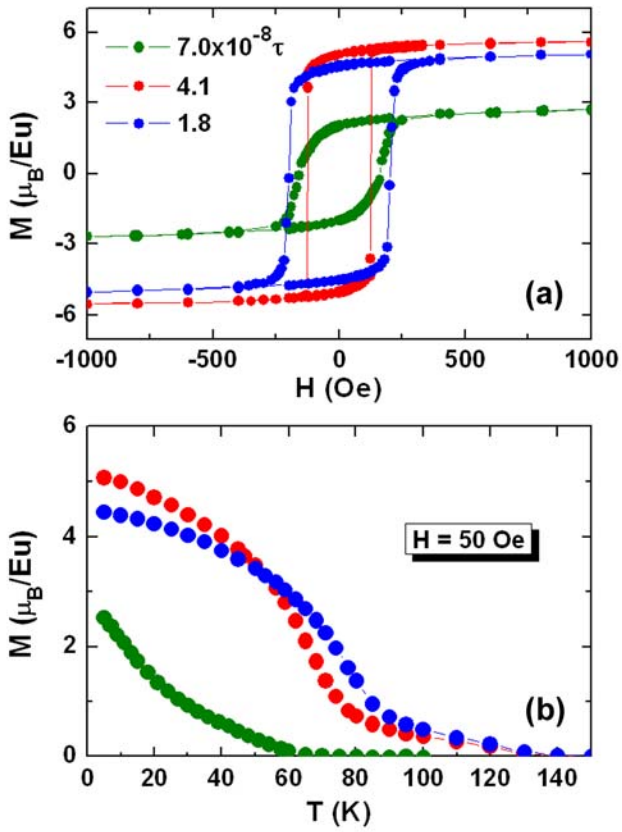

Fig.2 Magnetic properties of MBE deposited EuO thin films in three different oxygen pressures. (a) Magnetic hysteresis loops taken at 4.5 K; (b) temperature dependence of the magnetization, recorded under 50 Oe field-cooling.

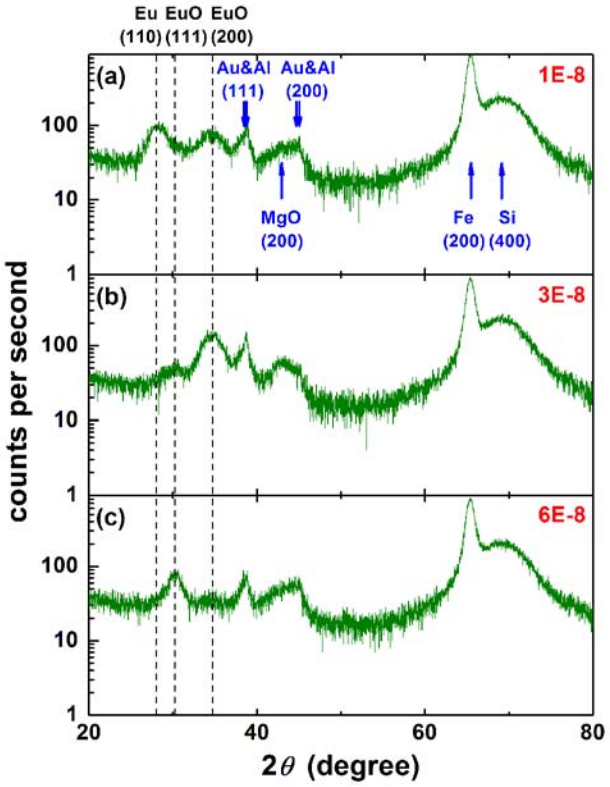

Fig.3 XRD pattern for a set of magnetic tunnel junction stacks (in nm): Si / 5 MgO / 20 Fe / 2 MgO / 3 EuO / 3 Y / 50 Al / 3 Cr / 5 Au. The stacks were epitaxial up to the MgO barrier, and polycrystalline starting from EuO layer. All growth parameters are identical except the oxygen pressure (labeled in red) in the EuO growth.

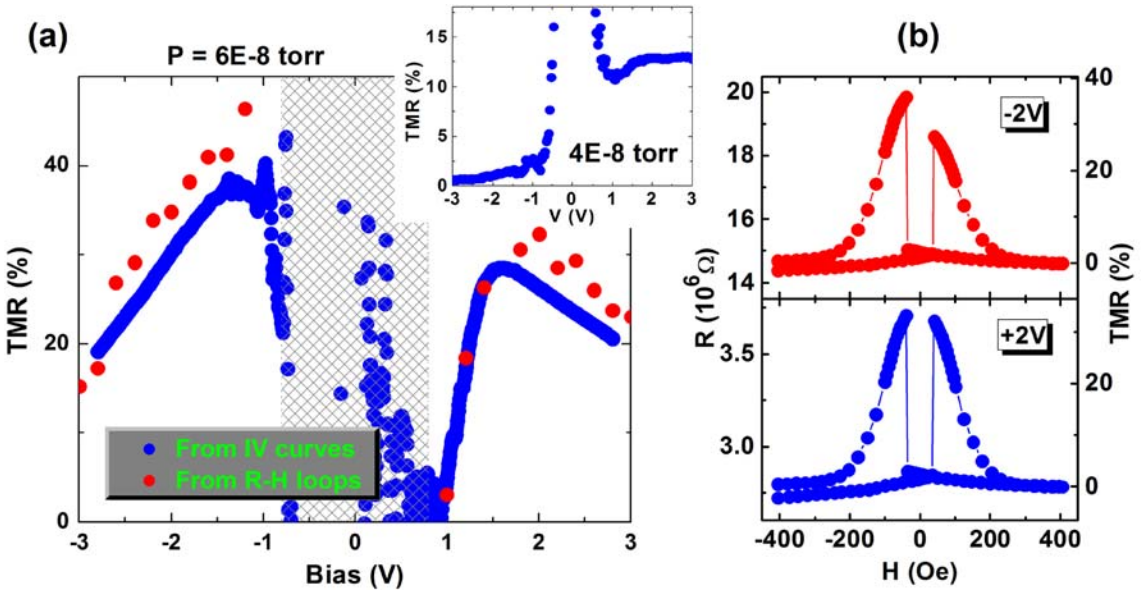

Fig.4 TMR behavior in a magnetic tunnel junction with EuO deposited at oxygen pressure of 6×10^{-8} torr. (a) TMR bias dependence. The blue data points are deduced from IV curves, and the red data points are from R vs H measurements. For bias voltages lower than 1 V (shaded area), high junction impedance prevented reliable measurement of TMR and led to the scattering of the data points. For comparison purpose, the inset shows bias dependence of a similar junction with EuO deposited at lower oxygen pressure (4×10^{-8} torr). (b) Examples of the typical R vs. H loops, for device deposited at 6×10^{-8} torr.

1 J.S. Moodera, L.R. Kinder, T.M. Wong, R. Meservey, Phys. Rev. Lett. **74**, 3273 (1995).
2 T. Miyazaki, N. Tezuka, J. Magn. Magn. Mater. **151**, 403 (1995).
3 R.A. de Groot, F.M. Mueller, P.G. Van Engen, K.H.J. Buschow, Phys. Rev. Lett. **50**, 2024 (1983).
4 J.M. de Teresa, A. Barthélémy, A. Fert, J.P. Contour, F. Montaigne, P. Seneor, Science **286**, 507 (1999).
5 M. Bowen, M. Bibes, A. Barthélémy, J.-P. Contour, A. Anane, Y. Lemaître, A. Fert, Appl. Phys. Lett. **82**, 233 (2003).
6 W.H. Butler, X.G. Zhang, T.C. Schulthess, J.M. MacLaren, Phys. Rev. B **63**, 054416 (2001).
7 J. Mathon, A. Umerski, Phys. Rev. B **63**, 220403(R) (2001).
8 S. Yuasa, T. Nagahama, A. Fukushima, Y. Suzuki and K. Ando, *Nat. Mat.* **3**, 868 (2004).

9 S.S.P. Parkin, C. Kaiser, A. Panchula, P.M. Rice, B. Hughes, M. Samant and S.-H. Yang, *Nat. Mat.* **3**, 862 (2004).
10 L. Esaki, P.J. Stiles, S. von Molnar, Phys. Rev. Lett. **19**, 852 (1967).
11 D.C. Worledge, T.H. Geballe, J. Appl. Phys. **88**, 5277 (2000).
12 P. LeClair, J.K. Ha, H.J.M. Swagten, J.T. Kohlhepp, C.H. van de Vin, W.J.M. de Jonge, Appl. Phys. Lett. **80**, 625 (2002).
13 G.X. Miao, M. Müller, J.S. Moodera, Phys. Rev. Lett. **102**, 076601 (2009).
14 G.X. Miao, M. Münzenberg, J.S. Moodera, Rep. Prog. Phys. **74**, 036501 (2011).
15 O.K. Anderson, T.L. Loucks, Phys. Rev. **167**, 551 (1968).
16 M.W. Shafer, T.R. McGuire, J. Appl. Phys. **39**, 588 (1968); K.Y. Ahn, Appl. Phys. Lett. **17**, 347 (1970); K. Lee, J.C. Suits, Phys. Lett. A **34**, 141 (1971).
17 A. Mauger, Phys. Status Solidi B **84**, 761 (1977).
18 G.X. Miao, Y.J. Park, J.S. Moodera, M. Seibt, G. Eilers, M. Münzenberg, Phys. Rev. Lett. **100**, 246803 (2008); G.X. Miao, J.Y. Chang, M.J. van Veenhuizen, K. Thiel, M. Seibt, G. Eilers, M. Münzenberg, J.S. Moodera, Appl. Phys. Lett. **93**, 142511 (2008).
19 C.W. Miller, J. Magn. Magn. Mater. 321, 2563 (2009).
20 G.X. Miao, J.S. Moodera, Appl. Phys. Lett. 94(18), 182504 (2009).
21 K. Kawaguchi , M. Sohma, Y. Oosawa, J. Magn. Magn. Mater. **148**, 80 (1995); Nobuyuki Iwata, Govind Pindoria, Tadataka Morishita, Kay Kohn, J. Phys. Soc. Jap. 69, 230 (2000).
22 A.G. Swartz, J. Ciraldo, JJI Wong, Y. Li, W. Han, T. Lin, S. Mack, J. Shi, D.D. Awschalom, R.K. Kawakami, Appl. Phys. Lett. 97 112509 (2010).
23 T.S. Santos, J.S. Moodera, Phys. Rev. B **69**, 241203(R) (2004).
24 T. Nagahama, T.S. Santos, J.S. Moodera, Phys. Rev. Lett. **99**, 016602 (2007).
25 G.X. Miao, J.S. Moodera, J. Appl. Phys. **106**, 023911 (2009).